ONLINE FIRST

REPORTS OF PRACTICAL ONCOLOGY AND RADIOTHERAPY

ISSN: 1507-1367

e-ISSN: 2083-4640

Dosimetry characteristics of polycarbonate/bismuth oxide nanocomposite for real-time application in the field of gamma-rays

Authors: Amir Veiskarami, Shahryar Malekie, Sedigheh Kashian, Suffian Mohamad Tajudin

DOI: 10.5603/rpor.101397

Article type: Research paper

Published online: 2024-07-04

Dosimetry characteristics of polycarbonate/bismuth oxide nanocomposite for real-time application in the field of gamma-rays

DOI: 10.5603/rpor.101397

Amir Veiskarami[1], Shahryar Malekie[2, 3], Sedigheh Kashian[2], Suffian Mohamad Tajudin[3]

[1]*Department of Medical Radiation Engineering, Science and Research Branch, Islamic Azad University, Tehran, Iran*

[2]*Radiation Application Research School, Nuclear Science and Technology Research Institute, Karaj, Iran*

[3]*School of Medical Imaging, Faculty of Health Sciences, Universiti Sultan Zainal Abidin (UniSZA), Terengganu, Malaysia*

Correspondence to: Shahryar Malekie, [2]Radiation Application Research School, Nuclear Science and Technology Research Institute, P.O. Box 31485-498, Karaj, Iran; e-mail: smaleki@aeoi.org.ir

Abstract

Background: Polymer-carbon nanostructures have previously been introduced for dosimetry of gamma rays with potential application in radiotherapy. In this research work, bismuth oxide (Bi_2O_3) nanoparticles were added into the amorphous polycarbonate (PC) matrix to enhance the probability of the photoelectric effect and dosimetry response in parallel.

Materials and methods: PC/Bi_2O_3 nanocomposites at concentrations of 0, 5, 20, 40, and 50 Bi_2O_3 wt% were fabricated via a solution method. Afterward, the samples were irradiated by gamma rays of cobalt-60 (^{60}Co) related to Picker V-9, and Therarton-780 machines at 30–254

mGy/min. Dosimetric characteristics were carried out including linearity, angular dependency, energy, bias-polarity, field size, and repeatability.

Results: Field emission scanning electron microscopy (FESEM) and transmission electron microscopy (TEM) analyses exhibited an appropriate dispersion state. The dosimeter response was linear at 30–254 mGy/min for the all samples. The 50 wt% sample exhibited the highest sensitivity at 4.61 nC/mGy. A maximum angular variation of approximately 15% was recorded in normal beam incidence. The energy dependence at two energies of 662 and 1250 keV was obtained as 0.7%. Bias-polarity for the 40, and 50 wt% samples at 400 V were measured as 15.9% and 9.0%, respectively. The dosimetry response was significantly dependent on the radiation field size. Also, the repeatability of the dosimeter response was measured as 0.4%.

Conclusions: Considering the dosimetry characteristics of PC-Bi_2O_3 nanocomposites, and appropriate correction factors, this material can be used as a real-time dosimeter for the photon fields at therapy level.

Key words: dosimetry; gamma rays; PC/Bi_2O_3 nanocomposite; dose rate; therapy level

Introduction

Recently, polymeric nanomaterials have attracted the attention of scientists regarding radiation protection [1], sensors [2], detectors, and dosimeters [3–12]. Knowing how radiation interacts with the matter is necessary in order to construct a radiation dosimeter. The right material should therefore be selected depending on the type of radiation. Polymers and organic compounds are examples of the materials utilized in ionizing radiation dosimetry. Recent studies have examined the gamma-ray dosimetric properties of the polymer/carbon nanostructures [6, 9]. The response of the polymer-nanocomposite dosimeter manifests as a change in the electric current flowing through the sample during irradiation. By calibrating this current in the Secondary Standard Dosimetry Laboratory (SSDL) in accordance with the known dose rate at a fixed reference condition, the dose rate of an unknown radiation field can then be determined. Bismuth oxide (Bi_2O_3) has been shown to behave as a significant metal oxide semiconductor with a band gap close to 2.91 eV at 300 K [13, 14]. Therefore, during the irradiation of the polymer-Bi_2O_3 nanocomposites, many electron holes can be generated. In order to gather the electric charges and convert them to an electric signal, a proper voltage should be applied on the nanocompopsite

during the irradiation. Irradiation causes recombination and charge trapping in the material, as shown by numerous investigations [15, 16]. In the previous study accomplished by the authors, this problem was solved by adding small amounts of graphene oxide into the HDPE/Bi_2O_3 nanocomposite for gamma rays of the cobalt-60 (^{60}Co) [17]. Polymer nanocomposites exhibit low sensitivity to gammarays due to their low densities. Therefore, to overcome this problem, bismuth oxide (Bi_2O_3) nanoparticles (with atomic number Z = 83 for Bi) are added to the polymer matrix. This can enhance the sensitivity for radiation detection and dosimetry by increasing the probability of photoelectric effect. Intaniwet et al. investigated the addition of heavy metal oxide nanoparticles in a semiconductor polymer to improve the detector sensitivity against the 17.5 keV X-rays [8]. Madani et al. used pure Poly(methyl methacrylate) (PMMA) and low-density polyethylene (LDPE) polymers to create an electric field between 1–5 kV/mm while simultaneously measuring the dosage rate of gamma rays [18, 19].

Due to the inclusions aggregation effects, the dispersion state of the nanoparticles in the polymer matrices is challenging, especially at greater volume fractions [20]. Polycarbonate (PC), an amorphous polymer, is a superior candidate for making homogenous nanocomposites [3]. It has been demonstrated that high levels of the polymer crystallinity can hinder the homogenous dispersion of the nanoparticles [21]. The polymer matrix was chosen to be PC, a thermoset polymer with an amorphous structure and repeat units of -CH_2-CH (C_6H_5). This amorphous polymer exhibits a suitable radiation hardness and superior breakdown voltage with regard to the aromatic structure of the PC [22–24]. In this work, a high-Z material, i.e. Bi_2O_3 nanopowder with a density of 8.9 g/cm^3, was also selected as a filler. Generally, nanoparticles at the dimension of nanometer exhibit extraordinary properties. One of these properties is the high value of the surface-to-volume ratio for nanoparticles. For a homogeneous dispersion state of the nanoparticles into the polymer matrix, which is a challenging issue during the fabrication process due to Van der Waals attractive force between the nanoparticles [5], the probability of the interaction of photon with the high-Z nanoparticles is increased.

In the previous work, a novel sensor for beta rays of a pure beta emitter radioactive source namely strontium-90 (^{90}Sr), with two energies of 546 keV and 2.28 MeV, was introduced [2]. Investigation of the effect of adding Bi_2O_3 nanoparticles on the dosimetry response of the PC/Bi_2O_3 nanocomposite was carried out using ^{90}Sr source [25].

In this work, the dependence of the dosimetric response of various concentrations of PC/Bi_2O_3 nanocomposites on linearity, angle, energy, bias polarity, field size, and reproducibility to gamma-ray measurements at the SSDL of Iran-Karaj was explored. The novelty of this work is using the PC/Bi_2O_3 nanocomposite material for dosimetry applications of the gamma rays of ^{60}Co at the therapy level, because in the SSDLs of some countries including Iran, ^{60}Co source is used to provide calibration services to hospitals.

Materials and methods

Sample preparation

In this experimental work, PC granules were supplied from the Iranian-Khuzestan petrochemical company with a density of 1.2 g/cm^3. Bi_2O_3 nanopowders with a density of 8.9 g/cm^3 and an average particle size of 90–210 nm were prepared by Sigma-Aldrich. Our earlier study contains specifics of the solution casting fabrication procedure [3]. In a summary, the polymer was dissolved using a hotplate magnetic stirrer, and the Bi_2O_3 nanoparticles were distributed throughout the polymer matrix using an ultrasonic probe. At 40°C, dichloromethane was used as the chemical solvent of the PC. The PC/Bi_2O_3 nanocomposites were then created using hot pressing with a fixed thickness of 1 mm and the same size (4 × 4 cm^2) at various concentrations of 0, 5, 20, 40, and 50 Bi_2O_3 wt%. Then, as depicted in Figure 1, a copper plate with a thickness of 100 μm was adhered to the sample using the silver paste in order to create the electrodes on both surfaces. The specifics of each sample are then given in Table 1.

Table 1. The nanofiller weight percentage (wt%)

Sample ID	**Polymer matrix**	**Bi_2O_3 wt%**
A_0	PC	0
A_5	PC	5
A_{20}	PC	20
A_{40}	PC	40
A_{50}	PC	50

Bi2O3 — bismuth oxide

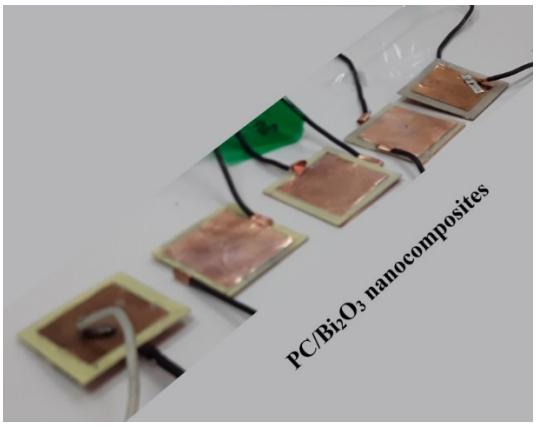

Figure 1. Preparation of the nanocomposite dosimeters

Instruments

As shown in Figure 2, the samples were subjected to gamma irradiation using the Picker-V9 and Theratron-780 ^{60}Co machines as well as the OB-85 Cesium-137 machine from the SSDL of Iran-Karaj at various source to surface distances (SSDs) in accordance with Table 2.

The initial average amount of dark current (current in the absence of exposure at a fixed voltage) was measured using an electrometer model Supermax Standard Imaging, in which the electrometer was set to zero for each measurement. Subsequently, under a fixed reference condition, the average current value as photocurrent was measured at the fixed voltage in time steps of 15 seconds.

(**A**) (**B**) (**C**)

Figure 2. Experimental setup, cobalt-60 (^{60}Co) machines models (**A**) Picker-V9; Theratron-780, (**B**) and cesium-137 (**C**) machine model OB-85 to irradiate the samples

Table 2. Amounts of source to surface distances (SSDs) for cobalt-60 (^{60}Co) machines in this research and corresponding dose rates at field size of 20 × 20 cm^2

SSD [cm]	Dose rate [mGy/min]	
	Picker-V9	**Theratron-780**
60	83.46	254.63
70	61.32	187.08
80	46.94	124.77
90	37.09	100.25
100	30.04	91.67

Dispersion of Bi_2O_3 nanoparticles

A fractured surface of the A_{50} sample, which contains 50 wt% Bi_2O_3 in the PC matrix, is depicted in Figure 3A using the field emission scanning electron microscopy (FESEM). Razi Metallurgy Research Centre in Iran conducted a FESEM analysis using the MIRA3TESCAN-XMU model. The figure demonstrates how evenly the Bi_2O_3 nanoparticles are distributed throughout the PC matrix. We expect to have a homogeneous material based on the FESEM image and the fact that polycarbonate is an amorphous polymer, which can result in a better dispersion state of the inclusions into the polymer matrix. High-density polyethylene, a semi-crystalline polymer containing 50 wt% Bi_2O_3, demonstrated agglomeration regions in the previous work [17].

Figure 3B illustrates how the transmission electron microscopy (TEM) analysis of the A_{50} sample revealed the dispersion state of the inclusions as well as the size of the Bi_2O_3 nanoparticles, in accordance with its manufacturer catalog (90-210 nm). Tehran University in Iran performed the TEM analysis using a model Philips CM30, Netherlands, at a voltage of 200 kV. Ultramicrotomy was carried out utilizing a Reichert-Jung Ultracut-E configured with a Diatome 45° diamond knife in order to conduct TEM studies.

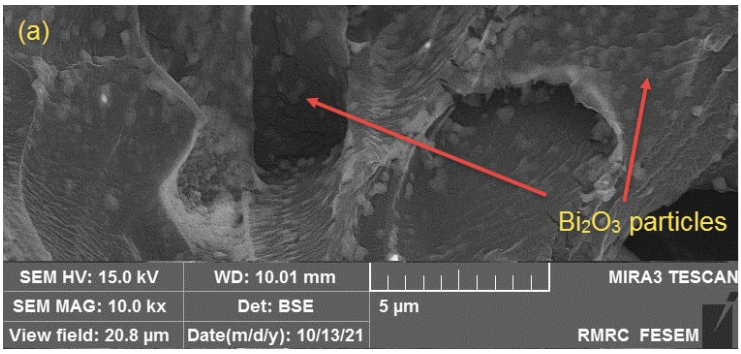

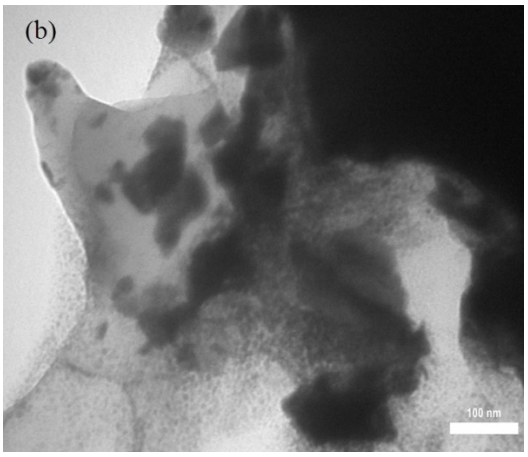

Figure 3. Analyses of field emission scanning electron microscopy (FESEM) (**A**) and transmission electron microscopy (TEM) (**B**) for the A_{50} sample containing 50 wt% of bismuth oxide (Bi_2O_3) in the polycarbonate (PC) matrix

Quantum efficiency

Greater attenuation coefficient of the material results in improved efficiency for detection and dosimetry purposes when radiation interacts with the matter at a given energy. Quantum efficiency (QE) is consequently described as [8]:

$$QE = \left(1 - e^{-\left(\frac{\mu}{\rho}\right)\rho x}\right) 100\% \quad (1)$$

where μ/ρ is the mass attenuation coefficient obtained from the photon cross-section database [26], ρ and x are the composite density and thickness, accordingly. In Table 3, the density and linear attenuation coefficients of the different loadings in the PC/Bi_2O_3 composite are exhibited. As can be seen from this table, with increasing the Bi_2O_3 wt%, the amounts of composite density and linear attenuation coefficients increase remarkably.

Table 3. Calculation of density, and linear attenuation coefficients for polycarbonate (PC)/bismuth oxide (Bi_2O_3) composite at 1250 keV using the XCOM program

Bi_2O_3 wt%	**$\rho_{Composite}$ [g/cm^3]**	**μ [cm^{-1}]**
0	1.20	0.0717
10	1.31	0.0781
20	1.45	0.0863
30	1.62	0.0963
40	1.84	0.1092

50	2.11	0.1250
60	2.50	0.1479

The density of a composite can be calculated as [27]:

$$\rho_c = \frac{1}{(W_f/\rho_f)+(W_m/\rho_m)} \quad (2)$$

In which ρ_C, ρ_f, and ρ_m are the densities of the composite, filler, and matrix, respectively; W_f, and W_m are the weight fractions of the filler and matrix, consecutively.

Results

Figure 4 displays the predicted quantum efficiencies of a 1 mm thick PC/Bi_2O_3 composite at 1250 keV with various Bi_2O_3 wt% using the MCNP code and XCOM program [26, 28]. Figure 4 indicates that as the concentration of the Bi_2O_3 particles rises from 0 to 50 wt%, the QE grows by a factor of 1.75. This figure shows that the highest efficiency at 1250 keV is 1.2% for the 50 wt% sample. However, this composite can be utilized as a promising material for monitoring the low-energy X-rays and photons at the diagnostic level, although the efficiency values for high-energy photons are relatively low. In general, the polymer matrix can be supplemented with high atomic number heavy metal oxide inclusions to increase the quantum efficiency of the composites [8].

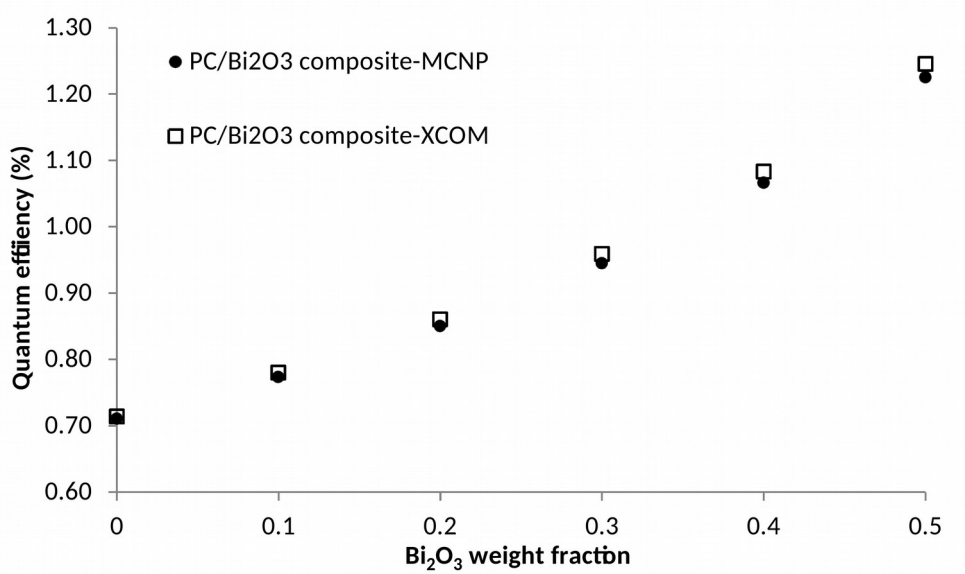

Figure 4. Calculated quantum efficiency of polycarbonate (PC)/bismuth oxide (Bi_2O_3) composite with a thickness of 1 mm at 1250 keV in different inclusion fractions

Bias-polarity dependence

Different readings between a positive and a negative bias voltage represent a polarity effect. In general, there is a polarity effect in ionization dosimeters, and the response requires a polarity correction factor. This effect is voltage dependent for ionization dosimeters and gets stronger as their volumes are smaller since the collecting volume undergoes greater relative fluctuations [29].

The current-voltage (I–V) plot for the two nanocomposites, namely A_{40} and $A_{50,}$ are shown in Figure 5 at the dose rate of 46 mGy/min in the SSD of 80 cm. The dosimetry response of the nanocomposite is shown to be roughly linear within the range of ± 1000 V. Generally, the optimum bias voltages for semiconductor detectors are close to the saturation region. This is not a difficult problem, because it is occasionally possible to operate the detector at a bias voltage that is below actual saturation without noticeably degrading the energy resolution when radiation of a single energy and type is present. After all, it is likely that the percentage of energy lost for each incident will be relatively consistent [30].

As shown in Figure 5, the standard deviation was measured as 2.4% at voltages of ± 1000 V. The maximum discrepancies for the A_{40} and A_{50} samples were measured as 15.4%, and 9.2% respectively, indicating the polarity dependence of the dosimeter response, especially at higher voltages. At 400 V, a common voltage for Geiger counters, the maximum discrepancies for the A_{40} and A_{50} samples, were measured as 15.9% and 9.0%, respectively. The observed discrepancy in Figure 5 may be attributed to a difference in the electron collection vs. hole collection, and charging up of the bulk, in which the polarity effect of the nanocomposite material leads to create the charges accumulated with positive and negative polarities [31]. Also, the geometry of the electrodes plays an important role during the investigation of the polarity sign on the dosimetry response of this real-time dosimeter. So, adding the guard electrode in the form of a ring around the anode can moderate this effect. Based on the I-V plot in Figure 5, it seems that behavior of this dosimeter obeys the proportional, in which with increasing the voltage, the collected charges increase accordingly.

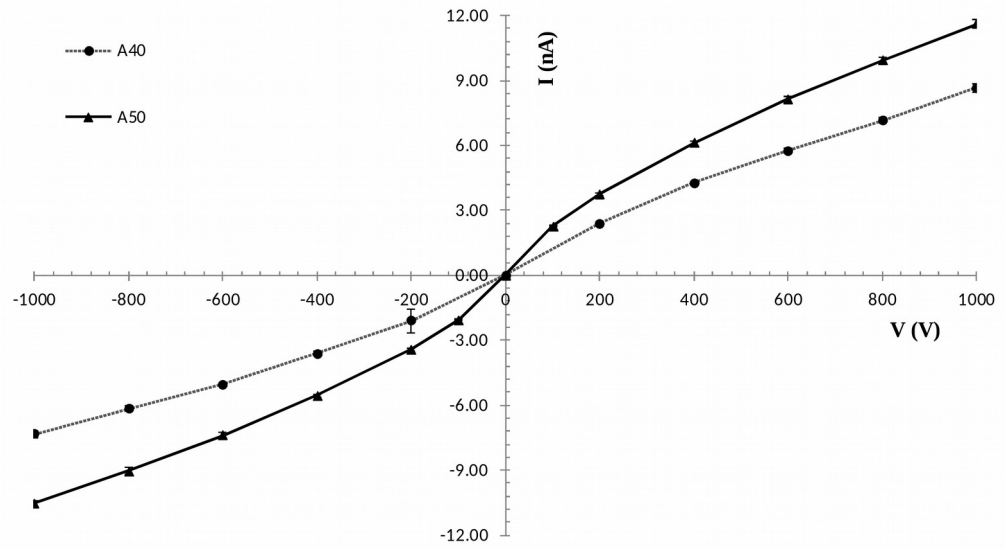

Figure 5. The current-voltage characteristic of the A_{40} and A_{50} samples at 46.85 mGy/min (2.4% standard deviation, 1σ).

Dose rate dependence

Figure 6 displays the average photocurrent as a function of dose rate for a variety of samples with a maximum standard deviation of 2.4% (1σ). As might be expected, higher gamma-ray dose rates result in the formation of more electron-hole pairs. The photocurrent will therefore be enhanced by increasing the dose rate.

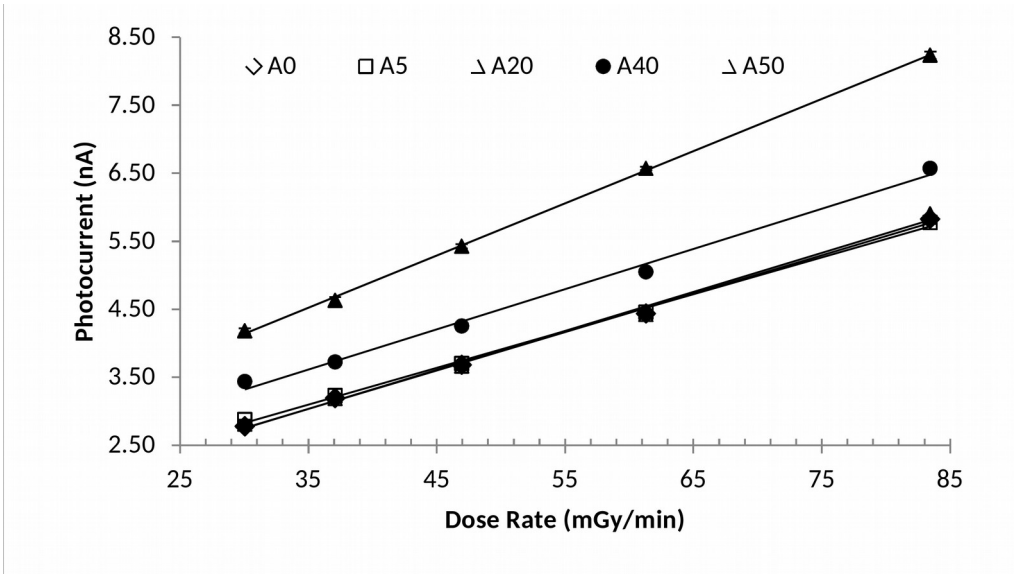

Figure 6. Average photocurrent vs. dose rate for various samples (2.4% standard deviation, 1σ).

In Figure 7, the dosimetry response of the PC/Bi_2O_3 nanocomposite at a fixed dose rate of 83.46 mGy/min is exhibited at various Bi_2O_3 wt%. Results show that increasing the reinforcement loading more than 40 wt% Bi_2O_3 leads to enhancing the photocurrent significantly. On the other hand, the quantum efficiency is enhanced based on Figure 4, indicating that more ionization has been achieved. Also, it seems that there is a threshold weight fraction of the Bi_2O_3 nanoparticles for enhancement of the dosimetry response in the polymer-nanocomposite, in which up to 20 wt %, the response is constant, but after 40 wt%, the response increases remarkably.

As shown in Figure 7, the photocurrent increases with the addition of Bi_2O_3 wt% into the polymer matrix, and there is no saturation in the dosimetry response. This behavior may be attributed to the amorphous structure of the polycarbonate, which results in a uniform dispersion state of the inclusions. Additionally, crystalline polymers, like high-density polyethylene (HDPE), face challenges in achieving uniform distribution of inclusions, resulting in agglomerations at higher levels of the reinforcement phase. This can lead to saturation in the dosimetry response at higher levels of the inclusions [17].

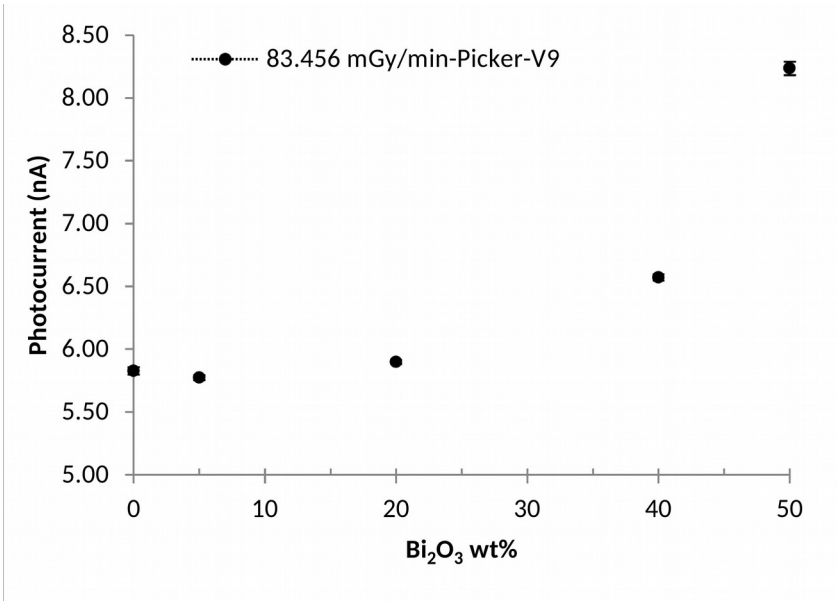

Figure 7. Dosimetry response for of polycarbonate (PC)/bismuth oxide (Bi_2O_3) nanocomposite at a fixed dose rate of 83.46 mGy/min

In a polymer-heavy metal oxide nanocomposite, some factors, such as thickness, heavy metal oxide wt%, applied bias voltage, and crystallinity of the polymer matrix can really be used to evaluate the sensitivity degree. It should be noticed that for therapeutic applications, the typical doses range from 12–97 Gy for [9, 32–34]. Also, in external radiotherapy, the total absorbed dose is fractionated over numerous sessions. As a result, for each session, the dose rate is in the range of mGy per minute. Thus, the dose rates studied in this research can be justified taking into account this issue.

Linearity response

One of the characteristics of a good dosimeter is the linearity of its response in the wide range of dose rates. By dividing the slope of the I-Dose rate plots (in Fig. 6) by the sensitive volume of each material (4 cm× 4 cm× 0.1 cm), the sensitivities of the samples were determined at a fixed voltage of 400 V [8]. Based on this method, the sensitivity of each sample is assessed in Table 4, in which R-squared (R^2) denotes regression linearity which is a measure of how closely the data points lie on the fitted line [35]. As shown in Table 4, the sensitivity of the A_{50} sample containing 50 wt% Bi_2O_3 in the PC matrix is 36.1% higher than the pure PC. It can be found that the sensitivity of the A_{50} sample is about ten times higher than that of the PIN diode dosimeter at the therapy level [36].

Table 4. Linear trendline in I-Dose rate plot for various samples irradiated with Picker-V9

Sensitivity [nC·mGy^{-1}]	**Sensitivity per sensitive volume [nC·mGy^{-1}·cm^{-3}]**	**R^2**	**Trendline**	**Sample**
3.39	2.1188	0.9977	y = 0.0565x + 1.0531	A_0
3.25	2.0325	0.9978	y = 0.0542x + 1.1999	A_5

3.44	2.1525	0.9949	y = 0.0574x + 1.0231	A_{20}
3.55	2.2163	0.9936	y = 0.0591x + 1.5454	A_{40}
4.61	2.8838	0.9995	y = 0.0769x + 1.8287	A_{50}

Signal to noise ratio

Figure 8 displays the signal-to-noise ratio (the difference between net current and dark current) of various samples at 400 V using the Picker-V9 gamma-rays. The A_{50} sample, namely 50 wt% PC/Bi_2O_3 nanocomposite, achieved the maximum signal-to-noise ratio. For the A_{50} sample, as illustrated in this figure, with increasing the dose rate ranging from 30–83 mGy/min, the signal-to-noise ratio will increase by 417 to 823 times compared to the dark current. The emission of secondary electrons, excitation, and ionization that occur when gamma-rays interact with the atomic structures of the nanocomposites is related to this process.

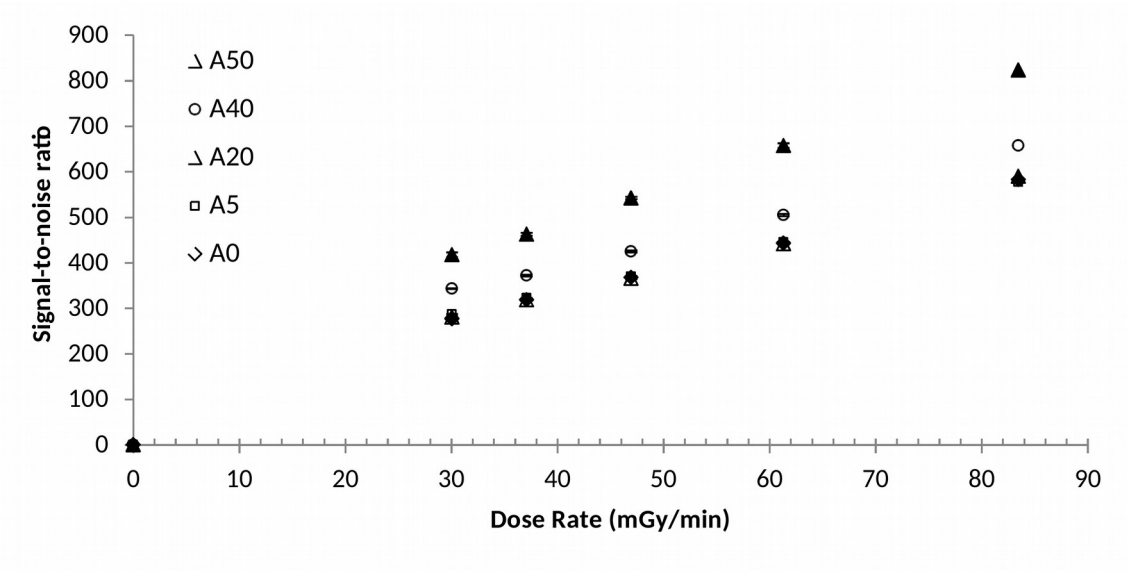

Figure 8. The signal-to-noise ratio of various samples at 400 V against the gamma-rays of Picker-V9 with a maximum standard deviation of 1.9% (1σ)

Since A_{50}, containing the 50 wt% PC/Bi_2O_3 nanocomposite, has the highest sensitivity of the investigated materials, as shown in Figure 9, the linearity response of this dosimeter was assessed using a different gamma-ray source called Theratron-780 with a dose rate roughly three times higher than the Picker-V9 at a same SSD. For the A_{50} sample, the dosimeter response exhibited a linear behavior, both using the Picker-V9 and the Theratron-780 machines with R^2 = 0.9995 and 0.9959, respectively.

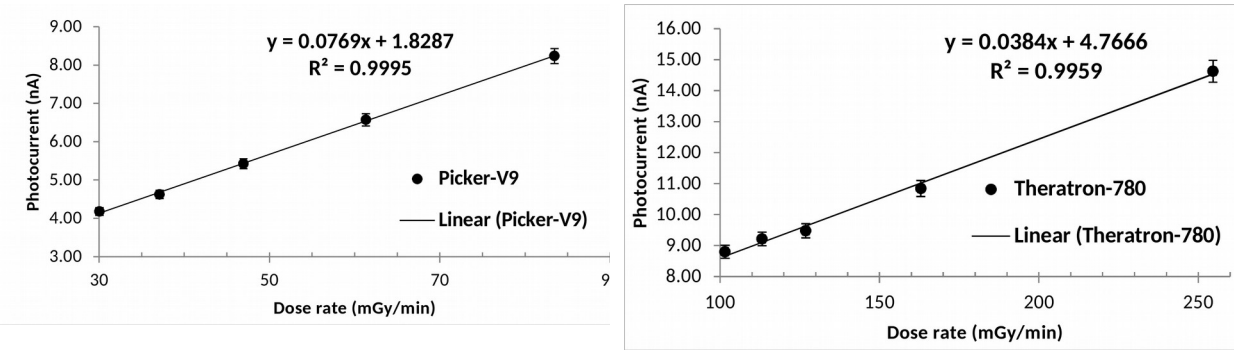

(**A**) (**B**)

Figure 9. Average photocurrent vs. dose rate for polycarbonate (PC)/bismuth oxide (Bi_2O_3) (50 wt%) nanocomposite using the two cobalt-60 (^{60}Co) machines: Picker-V9 (**A**), and Theratron-780 (**B**) (2.4% standard deviation, 1σ)

Time evolution

Figure 10 shows the time evolution of the dosimeter response for the A_{50} sample exposed to gamma rays using the Picker-V9 at SSD = 80 cm, field size = 20 × 20 cm^2, and a fixed dose rate of 46.85 mGy/h. The average dark current was less than 0.010 nA or 10 pA (current without exposure at a fixed voltage of 400 V or leakage current). Following that, the average current value at the fixed voltage of 400 V was measured as 6.58 nA at SSD=80 cm.

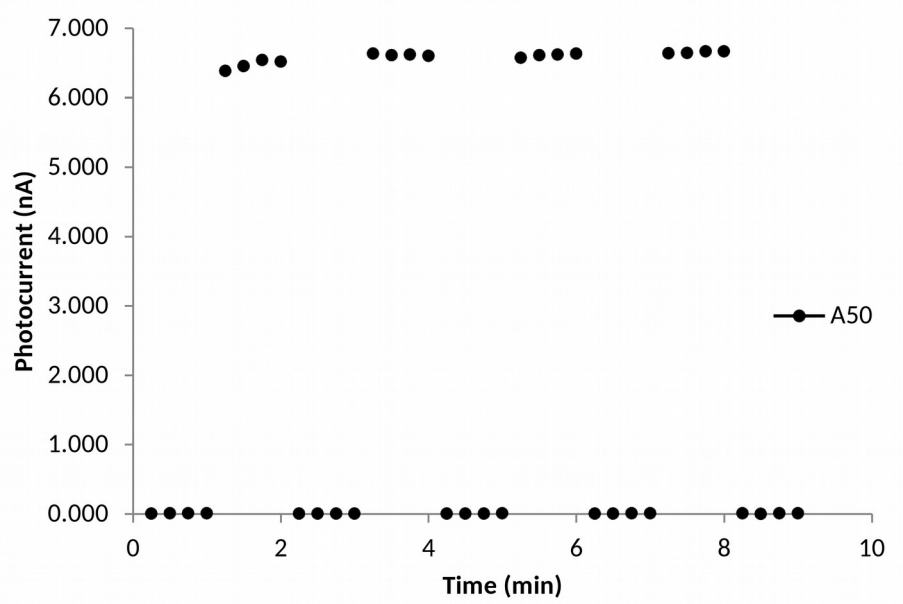

Figure 10. Time evolution of the dosimeter response at a fixed-dose rate of 46.85 mGy/h for the A_{50} sample

Angular dependence

One of the qualities of an excellent dosimeter is angular independence of the dosimetry response. To study the angular dependence, the Picker-V9 irradiation machine was used in the horizontal mode. So, the sample was mounted on a standard PMMA phantom with dimensions of 30 × 30 × 15 cm^3, in which a rotating plate including an electric motor was used.

Figure 11 depicts the angular dependence for the A_{50} sample irradiated by the Picker-V9 at SSD = 96 cm, dose rate = 30.67 mGy/min, and field size = 10×10 cm^2. The average photocurrent was measured at different angles in the range of θ = ±45°, which normalized angle at θ = 0°. The data was compared to 1/cos(θ) factor increase of the effective thickness penetrated by the radiation beam in Table 5. As observed from Table 5, and Figure 12, the signal gets stronger as θ increases in comparison with θ = 0° due to the increase of the thickness covered by the beam. By expanding eq. (1) based on the Taylor series, the amount of quantum efficiency can be expressed as:

$$QE \approx \left(\frac{\mu}{\rho}\right)\rho x - \frac{\left[\left(\frac{\mu}{\rho}\right)\rho x\right]^2}{2} + \ldots \qquad (3)$$

Since the amount of μ/ρ for the 50 wt% Bi_2O_3/PC composite was obtained 0.05926 cm^2/g through the XCOM program, so the second and subsequent sentences in eq. (3) can be ignored. Therefore, the quantum efficiency is exhibited as QE≈ (μ/ρ)·ρx≈ μx, where QE is proportional to x (thickness of the dosimeter) and linear attenuation coefficient subsequently at the specific energy. It can be concluded that the optimal thickness and the value of the filler concentration are important keys in this type of a dosimeter.

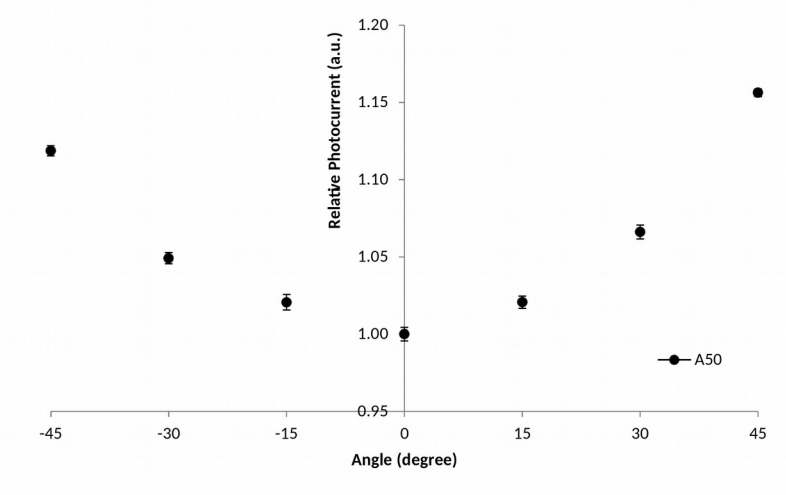

Figure 11. Variation of relative photocurrent of the A_{50} nanocomposite in different gamma-ray incident angles (2.2% standard deviation, 1σ)

Table 5. Comparison of the normalized signal with 1/cos(θ) factor increase of the effective thickness penetrated by the radiation beam

Angle(θ)	**Normalize ΔI(nA)**	**1/cos(θ)**
–45	1.12	1.41
–30	1.05	1.15
–15	1.02	1.04
0	1.00	1.00
15	1.02	1.04
30	1.07	1.15
45	1.16	1.41

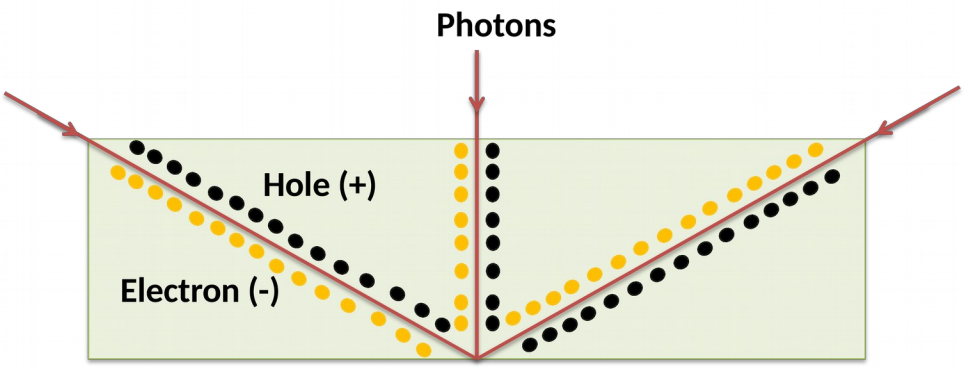

Figure 12. A schematic view of the incident photon beam angular ionization in the composite material.

This implies that the dosimeter response is dependent on the angle of the incident radiation [37]. As a result, the dosimeter response was around 15% more at 45° than at $\theta = 0°$. However, the angular dependency might be reduced at greater SSDs. As a result, the photocurrent generated in the nanocomposite is significantly influenced by the angle of the incident radiation.

Field size dependence

Figure 13 displays the radiation field size dependency of the A_{50} sample utilizing the Picker-V9 ranging from 10 × 10 cm^2 to 25 × 25 cm^2 at a fixed SSD = 80 cm. The figure exhibits a good agreement with the Kumar's findings for the PIN diode dosimeters against the therapeutic level gamma rays [36]. Figure 13 shows that the dosimeter response considerably enhances with increasing the field size. This can be explained by pointing out that because the sensitive volume of the dosimeter in this study is substantially greater than that of PIN diode dosimeter [36], when the size of the radiation field rises, the dosimeter will begin to read the scattered radiations around it. Therefore, to solve this problem, the field size dependency might be performed at the reference point inside a water phantom or tissue-equivalent plastic phantom subsequently. Also, the linearity of the dosimeter response over the various field sizes, even small fields, can promote the application of this dosimeter for the small field dosimetry.

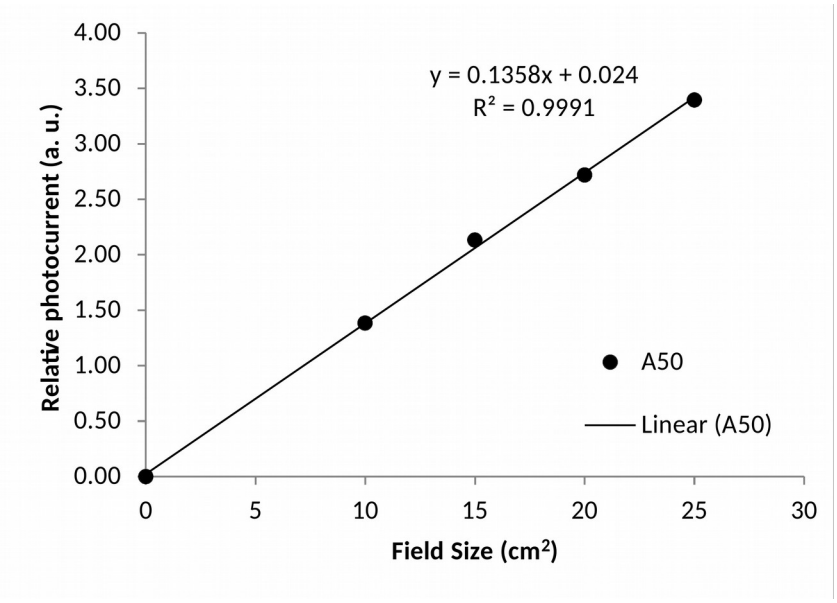

Figure 13. Variation of relative photocurrent vs. field size of A_{50} sample, (1.3% standard deviation, 1σ)

Energy dependence

An ideal dosimeter is less dependent on beam energy. Thus, to examine the energy-dependency of the dosimetry response of the A_{50} sample, two sources of ^{60}Co (average energy 1250 keV, Picker V9 machine, SSD = 389 cm) and ^{137}Cs (662 keV, OB-85 machine, SSD = 60 cm) at the same dose rate of 1.83 mGy/min were utilized. As can be seen from Figure 14, and Table 6, the dosimeter response exhibits a difference of 0.7%.

Table 6. Investigation of the energy dependence for A_{50} sample at the same dose rate of 1.83 mGy/min

Radiation source	**Energy [keV]**	**Photocurrent [nA]**
^{137}Cs	662	1.31 ± 0.03
^{60}Co	1250	1.30 ± 0.03

^{137}Cs — cesium-137; ^{60}Co — cobalt-60

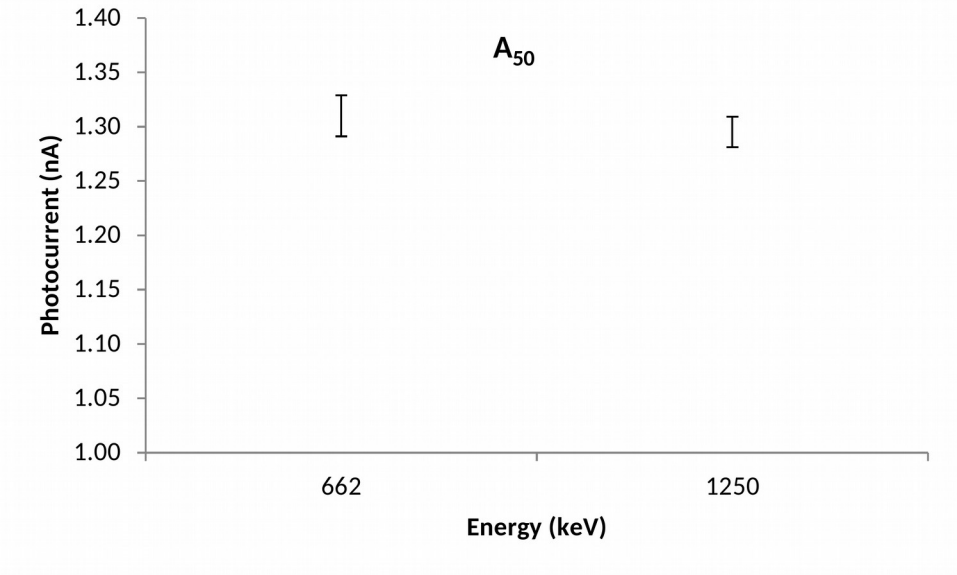

Figure 14. Investigation of the energy-dependency for A_{50} sample at the same dose rate of 1.83 mGy/min using cobalt-60 (^{60}Co), and cesium-137 (^{137}Cs)

Repeatability

Three consecutive relative readings of A_{40} sample at the same dose rate of 46.85 mGy/min (Picker V9 machine, SSD = 80 cm) are shown in Figure 15. The plot indicates that the response of the dosimeter is repeatable within 1.6%, which is substantially within the allowed range for therapeutic applications.

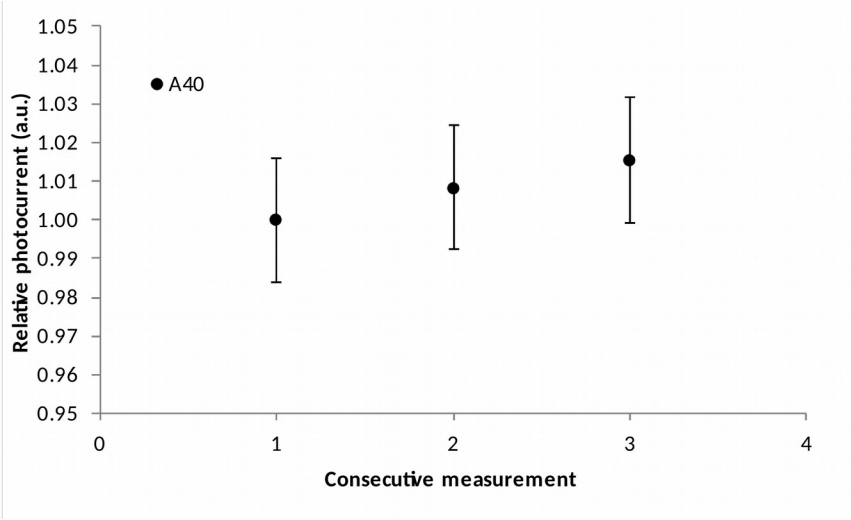

Figure 15. Repeatability investigation for the A_{40} sample (1.6% standard deviation, 1σ)

For a standard dosimeter, the condition of the charge particle equilibrium (CPE) should be provided. In fact, at the CPE depth, the absorbed dose and kerma (kinetic energy released per unit mass) is equal. In radiotherapy, to meet this requirement, in order to measure the absorbed dose, the ion chamber is placed inside a water phantom at the reference depth; otherwise, a buildup cap is applied. In this research, at the surface of the nanocomposite dosimeter, the amount of absorbed dose is lower than the air kerma. Therefore, in practice, a weaker signal is measured by the electrometer. It is possible to measure the amount of absorbed dose in an arbitrary medium. According to Burlin cavity relation, to access the absorbed dose in an arbitrary small medium, mass collision stopping power (S/ρ) is compared in both media, while for large ones, mass energy absorption coefficient (μ_{en}/ρ) is calculated consequently [38].

To evaluate the uncertainty in the measurement, type A and type B uncertainties were considered related to the random statistical and systematic errors, respectively. The uncertainty of type A (u_A) can be obtained through the repeatable measurements, while the uncertainty of type B (u_B) can be calculated via the precision and accuracy of the measurement instruments. Thus, the combined uncertainty (u_C) can be derived as [39]:

$$u_C = \sqrt{\left(\frac{u}{A}\right)^2 + \left(\frac{u}{B}\right)^2} \quad (4)$$

Taking into account the electric charge accumulation in the measurements carried out by the electrometer (model Supermax Standard Imaging) as 1.5% in the successive measurements as depicted in Fig. 15, thus, based on eq. (4), the total uncertainty was measured accordingly, which was applied to all figures.

Discussion

As demonstrated in this work, dosimetry characteristics of polycarbonate/bismuth oxide nanocomposites were examined in a ^{60}Co radiation field at the therapy level across the dose rate of 30–254 mGy/min at various concentrations of the Bi_2O_3 nanoparticles, namely 0, 5, 20, 40, and 50 wt%. The nanocomposites were made via a solution technique using the dichloromethane

solvent. The inclusions in the nanocomposites had a suitable dispersion condition, according to FESEM and TEM studies. Afterwards, various dosimetric characteristics were assessed, including linearity, angular dependence, energy dependence, bias-polarity dependence, field size effect, and repeatability for the samples. Results revealed that for all samples, the dosimeter response behaved linearly between 30–254 mGy/min. Among the other samples, the 50 wt% PC/Bi_2O_3 nanocomposite displayed the highest sensitivity as 4.61 nC/mGy. The maximum discrepancy of the dosimeter response at different angles of the incident beams was around 15% in comparison with the normal beam incidence ($\theta = 0°$). The energy dependence of the 50 wt% PC/Bi_2O_3 nanocomposite for gamma rays at energies of 662 and 1250 keV was studied. The variation in the dosimeter response for both energies at the same dose rate was assessed as 0.7%. Also, bias polarity experiments revealed that the dosimeter responses of the all samples were dependent on the bias voltage, in which the maximum discrepancies for the samples of 40 wt%, and 50 wt% at 400 V were measured as 15.9%, and 9.0%, respectively, which confirmed that a correction factor due to bias polarity should be taken into account. Results showed that the dosimetry response was greatly influenced by the radiation field size. Additionally, 1.6% repeatability was found in the dosimeter response.

Conclusion

The findings demonstrated that polycarbonate/bismuth oxide nanocomposites at high concentrations of the inclusions, specifically 50 wt%, may be employed as a real-time dosimeter applied for therapeutic level photon fields by taking into consideration various correction factors.

Conflict of interest

No declared.

Funding

No declared.

Author statement

A.V.: measurements, analysis and interpretation of data; S.M.: supervisor, conceptualization and writing; S.K.: adviser.

Acknowledgements

This work was extracted as part of a PhD thesis by Mr. A. Veiskarami, PhD student at Islamic Azad University, Science and Research Branch, Tehran. We express our appreciations to the people who helped us in conducting this research; particularly the NSTRI staff who make this study a success.

References

1. Hosseini MA, Malekie S, Kazemi F. Experimental evaluation of gamma radiation shielding characteristics of Polyvinyl Alcohol/Tungsten oxide composite: A comparison study of micro and nano sizes of the fillers. Nuclear Instruments and Methods in Physics Research Section A: Accelerators, Spectrometers, Detectors and Associated Equipment. 2022; 1026: 166214.
2. Safdari SM, Malekie S, Kashian M, et al. Introducing a novel beta-ray sensor based on polycarbonate/bismuth oxide nanocomposite. Sci Rep. 2022; 12: 2496.
3. Mehrara R, Malekie R, Saleh Kotahi SM. Introducing a novel low energy gamma ray shield utilizing Polycarbonate Bismuth Oxide composite. Sci Rep. 2021; 11: 10614.
4. Malekie S, Ziaie F. Study on a novel dosimeter based on polyethylene–carbon nanotube composite. Nuclear Instruments and Methods in Physics Research Section A: Accelerators, Spectrometers, Detectors and Associated Equipment. 2015; 791: 1–5, doi: 10.1016/j.nima.2015.04.031.
5. Malekie S, Ziaie F, Esmaeli A. Study on dosimetry characteristics of polymer–CNT nanocomposites: Effect of polymer matrix. Nuclear Instruments and Methods in Physics Research Section A: Accelerators, Spectrometers, Detectors and Associated Equipment. 2016; 816: 101–105, doi: 10.1016/j.nima.2016.01.077.
6. Malekie S, Ziaie F, Feizi S, et al. Dosimetry characteristics of HDPE–SWCNT nanocomposite for real time application. Nuclear Instruments and Methods in Physics Research Section A: Accelerators, Spectrometers, Detectors and Associated Equipment. 2016; 833: 127–133, doi: 10.1016/j.nima.2016.07.017.
7. Mosayebi A, Malekie S, Mosayebi S, et al. A feasibility study of polystyrene/CNT nano-composite as a dosimeter for diagnostic and therapeutic purposes. J Instrumentation. 2017; 12: P05012.
8. Intaniwet A, Mills CA, Shkunov M, et al. Heavy metallic oxide nanoparticles for enhanced sensitivity in semiconducting polymer x-ray detectors. Nanotechnology. 2012; 23: 235502, doi: 10.1088/0957-4484/23/23/235502, indexed in Pubmed: 22595835.
9. Mosayebi A, Malekie S, Rahimi A, et al. Experimental study on polystyrene-MWCNT nanocomposite as a radiation dosimeter. Radiat Phys Chem. 2019; 164: 108362, doi: 10.1016/j.radphyschem.2019.108362.

10. Kyatsandra S, Wilkins R. Total Ionizing Dose X-ray Radiation Effects on MWCNT/PMMA Thin Film Composites. IEEE Transactions on Nanotechnology. 2015; 14(1): 152–158, doi: 10.1109/tnano.2014.2374180.

11. Veiskarami A, Sardari D, Malekie S, et al. Computational prediction of electrical percolation threshold in polymer/graphene-based nanocomposites with finite element method. Journal of Polymer Engineering. 2022; 42(10): 936–945, doi: 10.1515/polyeng-2022-0101.

12. Malekie S, Ziaie F. A two-dimensional simulation to predict the electrical behavior of carbon nanotube/polymer composites. J Polymer Engin. 2017; 37: 205–210.

13. Bedoya Hincapie CM, Pinzon Cardenas MJ, Alfonso Orjuela JE, et al. Physical-chemical properties of bismuth and bismuth oxides: Synthesis, characterization and applications. Dyna. 2012; 79: 139–148.

14. Ho CH, Chan CH, Huang YS. The study of optical band edge property of bismuth oxide nanowires α-Bi 2 O 3, Optics Expr. 2013; 21: 11965–11972.

15. Un HI, Cheng P, Lei T. Charge-Trapping-Induced Non-Ideal Behaviors in Organic Field-Effect Transistors. Adv Materials. 2018; 30: 1800017.

16. Li H, Wang X, Chu H, et al. High performance resistive memory device based on highly stable layered CsPb2Br5 perovskite polymer nanocomposite. J Alloys Comp. 2022; 921: 166014.

17. Veiskarami A, Sardari D, Malekie S, et al. Evaluation of dosimetric characteristics of a ternary nanocomposite based on High Density Polyethylene/Bismuth Oxide/Graphene Oxide for gamma-rays. Sci Rep. 2022; 12(1): 18798, doi: 10.1038/s41598-022-23605-y, indexed in Pubmed: 36335163.

18. Madani N, Sardari D, Hosntalab M, et al. Effect of low dose gamma radiation on electric conductivity of LDPE and PMMA polymers. Engineering Solid Mechanics. 2020; 8: 31–40.

19. Madani N, Sardari D, Hosntalab M, et al. Real time dose rate meter for gamma radiation using LDPE and PMMA in presence of 1–5 kV/mm electric field. Radiat Phys Chem. 2018; 151: 164–168, doi: 10.1016/j.radphyschem.2018.06.002.

20. Kim J, Seo D, Lee B, et al. Nano-W Dispersed Gamma Radiation Shielding Materials. Adv Engin Materials. 2014; 16(9): 1083–1089, doi: 10.1002/adem.201400127.

21. Kaur J, Lee J, Shofner M. Influence of polymer matrix crystallinity on nanocomposite morphology and properties. Polymer. 2011; 52(19): 4337–4344, doi: 10.1016/j.polymer.2011.07.020.

22. Chen J, Huang X, Jiang P, et al. Protection of SEBS/PS blends against gamma radiation by aromatic compounds. J Appl Polymer Sci. 2009; 112(2): 1076–1081, doi: 10.1002/app.29552.

23. Gurkalenko YA, Eliseev D, Zhmurin P, et al. The plastic scintillator activated with fluorinated hydroxyflavone. Function Mat. 2017; 24: 244–249.

24. Mark JE. Physical properties of polymers handbook. Springer 2007.

25. Malekie S, Kashian S, Safdari SM, et al. Effect of reinforcement phase loading on the dosimetry response of a Polycarbonate/Bismuth Oxide nanocomposite for beta particles. Radiat Phys Engineering. 2022; 3: 11–15.

26. Berger MJ, Hubbell JH, Seltzer SM et al. 2011 XCOM: Photon Cross Sections Database, National Institute of Standards and Technology, USA, http://physics.nist.gov/PhysRefData/Xcom/Text/XCOM.html.

27. Rahman A, Singh A, Karumuri S. et al. Graphene reinforced silicon carbide nanocomposites: processing and properties. In: Tandon G. ed. Composite, Hybrid, and Multifunctional Materials. Vol. 4. Springer 2015: 165–176.

28. Briesmeister J. MCNP4C-Monte Carlo N-Particle transport code system version 4C. Los Alamos National Laboratory, Los Alamos 2005.

29. Wegener S, Sauer OA. Electrometer offset current due to scattered radiation. J Appl Clin Med Phys. 2018; 19(6): 274–281, doi: 10.1002/acm2.12458, indexed in Pubmed: 30298980.

30. Knoll, GF. Radiation Detection and Measurement. 4th ed. John Wiley & Sons, Inc, Michigan 2010.

31. Akbas A, Donmez Kesen C, Koksal C, et al. Surface and buildup region dose measurements with Markus parallel-plate ionization chamber, GafChromic EBT3 film, and MOSFET detector for high-energy photon beams. Bilge, Surface and buildup region dose measurements with Markus parallel-plate ionization chamber, GafChromic EBT3 film, and MOSFET detector for high-energy photon beams, Advances in High Energy Physics. Adv High Energy Phys; 2016.

32. Scott J, Berglund A, Schell M, et al. A genome-based model for adjusting radiotherapy dose (GARD): a retrospective, cohort-based study. Lancet Oncol. 2017; 18(2): 202–211, doi: 10.1016/s1470-2045(16)30648-9, indexed in Pubmed: 27993569.

33. Fachin A, Mello S, Sandrin-Garcia P, et al. Gene Expression Profiles in Radiation Workers Occupationally Exposed to Ionizing Radiation. J Radiat Res. 2009; 50(1): 61–71, doi: 10.1269/jrr.08034, indexed in Pubmed: 19218781.

34. Manning G, Kabacik S, Finnon P, et al. High and low dose responses of transcriptional biomarkers in*ex vivo*X-irradiated human blood. Int J Radiat Biol. 2013; 89(7): 512–522, doi: 10.3109/09553002.2013.769694, indexed in Pubmed: 23362884.

35. Aggarwal R, Ranganathan P. Common pitfalls in statistical analysis: Linear regression analysis. Perspect Clin Res. 2017; 8(2): 100–102, doi: 10.4103/2229-3485.203040, indexed in Pubmed: 28447022.

36. Kumar R, Sharma SD, Philomina A, et al. Dosimetric Characteristics of a PIN Diode for Radiotherapy Application. Technol Cancer Res Treat. 2014; 13(4): 361–367, doi: 10.7785/tcrt.2012.500388, indexed in Pubmed: 24325130.

37. Saavedra MS. Novel Organic Based Nano-composite Detector Films: The Making and Testing of CNT Doped Poly(acrylate) Thin Films on Ceramic Chip Substrates. Department of Physics, University of Surrey, Guildford, Surrey 2005: 37.

38. Attix FH. Introduction to radiological physics and radiation dosimetry. Wiley-VCH Verlag GmbH & Co. KGaA, Weinheim, Madison, Wisconsin 2004.

39. International Standards Organization. Guide to the Expression of Uncertainty in Measurement. ISO, Geneva 1993.